JOURNAL OF GEOPHYSICAL RESEARCH, VOL. 115, D03205, doi:10.1029/2009JD012108, 2010

Influence of parameterized ice habit on simulated mixed phase Arctic clouds

Alexander Avramov[1,2] and Jerry Y. Harrington[1]

Received 23 March 2009; revised 2 October 2009; accepted 14 October 2009; published 12 February 2010.

[1] The phase partitioning of cloud mass between liquid and ice in mixed phase clouds and its dependence on ambient ice nuclei (IN) concentrations and ice habit parameterizations is explored in this paper. Single-layered and multilayered cloud systems observed during the Mixed-Phase Arctic Cloud Experiment were simulated with a cloud-resolving model. The model used a two-moment (mass and number concentration) microphysical scheme with ice crystal habit parameterized by mass and fall speed relationships and IN prediction scheme that accounts for depletion of IN through nucleation scavenging. The mixed phase cloud simulations show a strong sensitivity to the ambient deposition/condensation freezing IN concentrations, which is similar to some prior studies. This sensitivity depends on the mass, fall speed, and capacitance relationships used to parameterize crystal habit and vapor growth: Mass and fall speed relationships associated with compact, high-density crystals produce clouds with a weaker sensitivity to ambient IN concentrations, whereas more extreme crystal shapes (e.g., dendrites) produce clouds with strong IN concentration sensitivity. This sensitivity also affects the number of liquid layers (from 1 to 5) predicted for the multilayer case. The strength of the vapor growth rates and the crystal fall speeds appear to be of roughly equal importance for determining the strength of mixed phase cloud sensitivity to ice concentrations.

Citation: Avramov, A., and J. Y. Harrington (2010), Influence of parameterized ice habit on simulated mixed phase Arctic clouds, *J. Geophys. Res.*, *115*, D03205, doi:10.1029/2009JD012108.

1. Introduction

[2] Mixed phase stratus clouds are prevalent in the Arctic during the winter and transition seasons [*Curry et al.*, 1996; *Intrieri et al.*, 2002]. Because of the lower equilibrium vapor pressure of ice as compared to liquid, ice crystals in mixed phase clouds grow at the expense of the cloud droplets (Wegener-Bergeron-Findeisen process, hereafter Bergeron process [*Pruppacher and Klett*, 1997, pp. 548–549]). Subsequent ice precipitation may then cause the complete glaciation and dissipation of the cloud. Nevertheless, the liquid phase is commonly found in Arctic clouds [*Pinto*, 1998; *Hobbs and Rangno*, 1998; *Prenni et al.*, 2007] to temperatures as low as −31°C [e.g., *Hobbs and Rangno*, 1998]. These cloud systems can persist from a few days to a couple of weeks. Capturing this persistence poses modeling challenges and is important in part because the radiatively important liquid phase affects the surface energy budget [*Shupe and Intrieri*, 2004; *Prenni et al.*, 2007] and, consequently, the freezing and melting rate of the Arctic sea ice [*Jiang et al.*, 2000; *Francis et al.*, 2005; *Kay et al.*, 2008].

[3] Regional and climate models have difficulties simulating the persistence of mixed phase clouds (Arctic Climate Model Intercomparison Project [*Curry and Lynch*, 2002]). Many models are able to predict liquid water paths similar to those observed during the summer season, but not during the winter when many models predict little liquid water. Discrepancies like these cannot be attributed to oversimplified cloud microphysical parameterizations alone as more advanced schemes can perform worse [*Prenni et al.*, 2007].

[4] At present, how mixed phase Arctic clouds can maintain supercooled liquid for extended periods of time is not completely understood, though several hypotheses have been advanced. Small crystal sizes at cloud top [*Rauber and Tokay*, 1991], strong dynamic forcing [*Korolev and Isaac*, 2003; *Korolev*, 2007], and low ambient ice nuclei (IN) concentrations [e.g., *Pinto*, 1998; *Harrington et al.*, 1999; *Jiang et al.*, 2000] have all been advanced as reasons for mixed phase cloud persistence though it seems likely that all of these mechanisms work in tandem. For instance, *Harrington et al.* [1999] hypothesized that mixed phase clouds are maintained through a balance between liquid water production resulting from cloud top radiative cooling and turbulent fluxes of vapor from below in conjunction with ice sedimentation. *Harrington et al.* [1999] suggested that this balance depends on the low average ambient deposition/condensation IN concentrations in the Arctic (<1 L^{-1} [*Bigg*, 1996; *Rogers et al.*, 2001]). This balance, however, also depends on IN removal by sedimentation [*Harrington and Olsson*, 2001] and possibly on the crystal habit assumed in the model [*Harrington et al.*, 1999].

[1]Department of Meteorology, Pennsylvania State University, University Park, Pennsylvania, USA.
[2]Now at NASA Goddard Institute for Space Studies, New York, New York, USA.

0148-0227/10/2009JD012108$09.00

[5] The rapid removal of deposition/condensation freezing IN tends to produce clouds with ice water contents (IWCs) and ice concentrations that are too low in comparison to observations [e.g., *Morrison et al.*, 2005; *Fridlind et al.*, 2007; *Morrison et al.*, 2008] This has led to the hypothesis that IN-rich air from above the boundary layer is entrained leading to continual ice production [e.g., *Carrio et al.*, 2005]. Indeed, *Avramov and Harrington* [2006] showed that mesoscale circulations along the northern Alaska coastline bring IN-rich air down to the boundary layer leading to a band of continuous precipitation along the coast, which is similar to observations. Regardless, *Avramov and Harrington*'s [2006] and *Prenni et al.*'s [2007] simulations produce IWCs and ice concentrations that are too low, and none of the observed precipitation bursts [e.g., *McFarquhar et al.*, 2007; *Fridlind et al.*, 2007].

[6] Efforts to increase both the IWC and ice concentration have focused on nucleation mechanisms. *Morrison et al.* [2005] suggest that the persistence of, and continual production of ice in, Arctic mixed phase clouds involves a self-regulating negative feedback due to drop freezing by contact nucleation. In contradistinction, *Avramov and Harrington* [2006] could not produce significant IWCs by contact nucleation unless the contact IN concentrations were as high as those reported by *Young* [1974], which are considered to be too large [e.g., *Meyers et al.*, 1992]. It is important to note that the *Avramov and Harrington* [2006] case was at least 3°–6° warmer, with a larger liquid water path (LWP), than the case simulated by *Morrison et al.* [2005].

[7] The importance of alternative nucleation mechanisms in mixed phase clouds has been extensively analyzed by *Fridlind et al.* [2007]. In order to maintain liquid while obtaining realistic ice concentrations, and ice precipitation bursts, *Fridlind et al.* [2007] parameterized two relatively controversial nucleation mechanisms. The first mechanism, "evaporation nucleation," hypothesizes that a fraction of all evaporating supercooled drops freeze [*Cotton and Field*, 2002]. The second hypothesis, "evaporation IN," suggests that IN are released during drop evaporation [*Rosinski and Morgan*, 1991]. *Fridlind et al.* [2007] show that these two mechanisms can produce liquid and ice amounts that consistently match observations.

[8] While most prior studies focus primarily on ice nucleation and ice concentrations, it is also feasible that how ice habit is parameterized could influence the simulated structure of mixed phase clouds. The Bergeron process depends not only on the ice concentration but also on the in-cloud residence time and vapor growth rate, both of which depend on habit and size [e.g., *Chen and Lamb*, 1994; *Fukuta and Takahashi*, 1999]. Indeed, in a simplified example *Harrington et al.* [1999] showed that different habits can have an impact on simulated mixed phase clouds. Moreover, many models use different parameterizations for ice habit, which may lead to differences in the model results. In this paper, we examine the influence that parameterized ice habit has on the evolution of mixed phase Arctic stratus.

2. Case Description

[9] We focus on two periods from the Mixed-Phase Arctic Cloud Experiment (M-PACE [*Verlinde et al.*, 2007]), the period from 1200 UT on 5 October to 1200 UT on 8 October (case A) and the period from 1700 UT on 9 October to 0500 UT on 10 October 2004 (case B). Case B was a single-layer mixed phase cloud [*Klein et al.*, 2009] whereas case A had multiple (four to five) transient liquid layers with ice crystals falling between them [*Morrison et al.*, 2009]. Surface-based measurements were taken for both cases at Barrow, Alaska, and at Oliktok point (~220 km east of Barrow), and in situ aircraft measurements were also taken [*McFarquhar et al.*, 2007].

[10] During case A (5–8 October 2004) a high-pressure center was developing over the sea ice to the northeast of the northern Alaska coast (Figure 1a). A small, midlevel low-pressure center moved east to west along the northern coast, bringing midlevel and upper level moisture that produced multilayer mixed phase clouds [*Verlinde et al.*, 2007]. The midlevel disturbance, and the cloud layers, dissipated on 7 October, but upper layer clouds reappeared later on 8 October. During case B (9–10 October), high pressure over the sea ice together with a surface Aleutian low produced northeasterly winds that moved cold air (approximately −20°C) from the sea ice over the relatively warm ocean (Figure 1b). This flow produced single-layer mixed phase boundary layer clouds and rolls [*Verlinde et al.*, 2007, Figure 3].

3. Model Description

[11] The model used in this study is the Colorado State University version of the Regional Atmospheric Modeling System (RAMS@CSU [*Cotton et al.*, 2003]) with two-moment bulk microphysics [*Walko et al.*, 1995; *Meyers et al.*, 1997]. The microphysical model has seven hydrometeor categories: cloud droplets, rain, pristine ice, snow, aggregates, graupel, and hail. Both mixing ratio and number concentration are predicted for all categories, except cloud droplets, for which the number concentration is prescribed. Pristine ice and snow categories are primarily vapor grown and together allow for a bimodal ice crystal size distribution [*Harrington et al.*, 1995]. The pristine ice category represents small crystals (mean maximum dimension $\equiv \overline{D} < 125$ μm) into which ice nucleates. Snow is defined as larger ice crystals (125 μm $< \overline{D} <$ 10 mm) that grow by vapor deposition and a small amount of riming. Ice is converted between snow and pristine ice by vapor diffusion. Aggregates form by collection between pristine ice, snow, and aggregates. Graupel is assumed to be spherical and is formed by riming or partial melting of pristine ice, snow, and aggregates. The hail category is not used in this study.

[12] Pristine ice crystals are formed by homogeneous and heterogeneous nucleation. Three of the four heterogeneous nucleation modes (that require IN) are explicitly present in the model: condensation/deposition freezing and contact freezing, whereas immersion freezing is assumed to be implicit in the deposition/condensation freezing (hereafter deposition freezing) parameterization of *Meyers et al.* [1992] and possibly in the IN measurements from M-PACE [*Prenni et al.*, 2007; P. DeMott, personal communication, 2006]. The number of IN acting in the deposition freezing mode is parameterized as a function of ice supersaturation following *Meyers et al.* [1992],

$$N_i = \exp(a + bS_i), \tag{1}$$

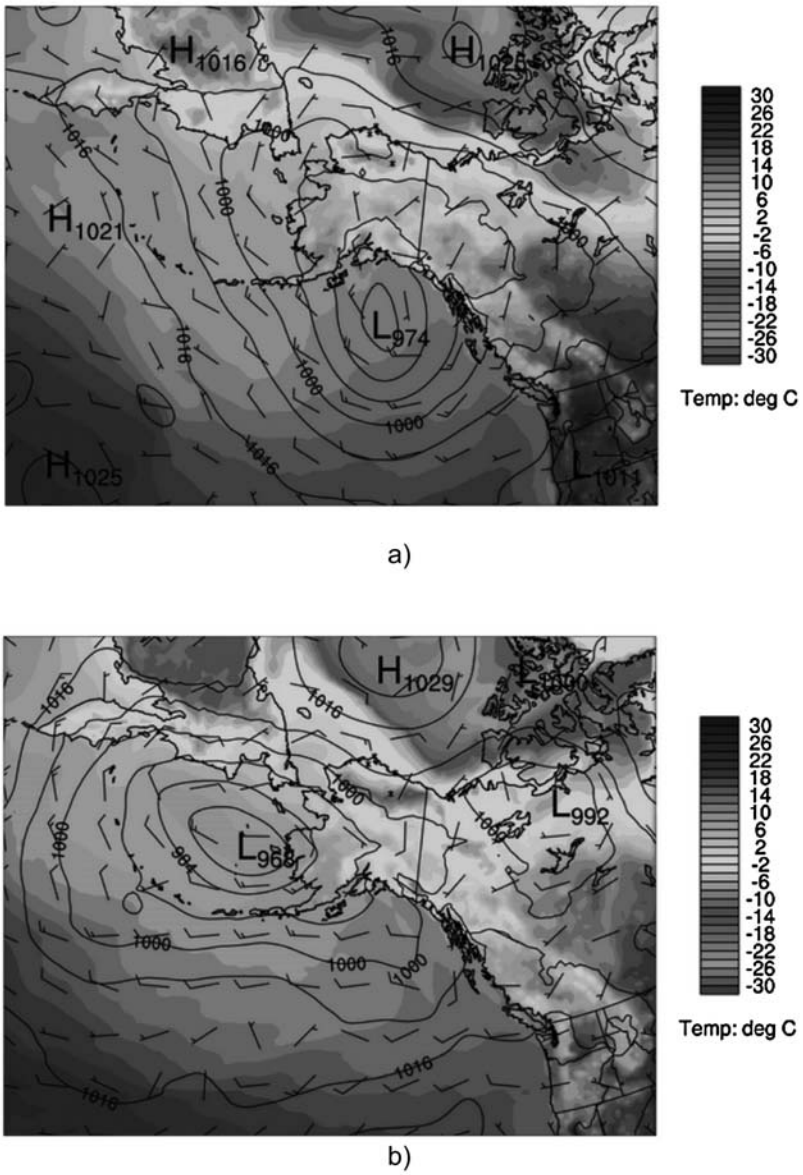

Figure 1. ETA surface analysis valid for (a) 0000 UTC 6 October 2004 and (b) 0000 UTC 10 October 2004. Air temperature (shaded, °C), mean sea level pressure (contoured, hPa), and surface wind (barbs, 5 m s^{-1}) are shown.

where N_i is the number of nucleated crystals (L^{-1}), S_i is the ice supersaturation (%), and a and b are empirically derived coefficients. The coefficients in equation (1) were modified using M-PACE IN data [see *Prenni et al.*, 2007]. The modified parameterization predicts IN concentrations of $\sim$0.15 L^{-1} at water saturation for our cases (see sections 4–6), which is consistent with other Arctic IN measurements [e.g., *Bigg*, 1996; *Rogers et al.*, 2001] and a factor of 26 lower than the standard Meyers parameterization. Contact nucleation is computed following *Meyers et al.* [1992], except that the contact IN concentration is arbitrarily reduced by a factor of 26 for consistency with the reduction in deposition IN. The concentrations of IN are prognosed in our simulations through a method of nucleation scavenging. This method assumes that equation (1) provides an estimate of the number of available IN. Once activated, IN are removed from the number of available IN. This method assumes that all activated IN are removed by precipitation, which overestimates the effects of nucleation scavenging [*Avramov and Harrington*, 2006; *Prenni et al.*, 2007].

[13] The parameterized ice habit is important for simulated mixed phase cloud evolution because liquid depletion by the ice crystals depends on the vapor growth rate and fall speed, both of which depend on habit. The fall speed of the crystals is parameterized following *Mitchell* [1996],

$$v_t = \alpha_{vt} D^{\beta_{vt}}, \tag{2}$$

where D is the crystal maximum dimension and α_{vt} and β_{vt} are empirically derived coefficients that differ for each

crystal habit. The vapor growth rate for a single crystal is [cf. *Walko et al.*, 1995; *Pruppacher and Klett*, 1997, p. 547]

$$\frac{dm}{dt} = 2\pi D S \psi f_{\mathrm{Re}}(v_t)(\rho_{va} - \rho_{vsh}), \tag{3}$$

where ψ is the vapor diffusivity, m is crystal mass, ρ_{va} is the ambient vapor density, ρ_{vsh} is the ice equilibrium vapor density, S is the shape factor that is defined as $S = C/D$ with C being the crystal capacitance, and f_{Re} is the ventilation coefficient that depends on the fall speed [*Cotton et al.*, 1982],

$$f_{\mathrm{Re}} = \left[1 + 0.229\left(\frac{v_t D}{V_k}\right)^{1/2}\right], \tag{4}$$

where V_k is the kinematic viscosity of the air. The shape factor (S) is fixed during a simulation even though it changes with crystal aspect ratio [e.g., *Chen and Lamb*, 1994]. Prognosis of the crystal mass requires a functional relationship between mass and size. Many models use a mass relationship like that given by *Mitchell* [1996],

$$m = \alpha_m D^{\beta_m}, \tag{5}$$

where α_m and β_m are empirically derived coefficients for each habit. As a consequence of the mass relationship and crystal capacitance, different crystal shapes have different growth characteristics. In general, more extreme aspect ratios lead to a larger capacitance, and faster vapor growth [e.g., *Chen and Lamb*, 1994]. For instance, dendrites grow faster than hexagonal plates because of the greater capacitance and extreme aspect ratio of the dendrites [e.g., *Chen and Lamb*, 1994; *Fukuta and Takahashi*, 1999; *Sheridan*, 2008; *Sheridan et al.*, 2009].

4. Model Setup and Simulation Design

[14] The RAMS model was configured as a 2-D cloud-resolving model for the recent M-PACE intercomparison studies [*Klein et al.*, 2009; *Morrison et al.*, 2009]. The computational domain has 150 horizontal grid points with 1 km spacing and 72 vertical grid points with 25 m spacing in the boundary layer, stretching to 1000 m at the domain top. The model is initialized with a prescribed sounding along with imposed large-scale forcing and surface fluxes developed specifically for the M-PACE intercomparison studies. The lower boundary is assumed to be snow-covered land (case A, multilayer) or ocean (case B, single layer). The large-scale forcing was constant in case B and time varying in case A. The simulation duration of case A is 72 h and case B is 12 h, with a 2-s time step; the lateral boundary conditions for both cases were periodic. A detailed description of the case studies is given by *Morrison et al.* [2009] for case A and by *Klein et al.* [2009] for case B.

[15] Both contact and deposition/condensation freezing IN are prognosed in the simulations. The IN concentration is advected by the wind, diffused by turbulence, and depleted when ice crystals nucleate and precipitate out of the atmosphere. No surface sources, IN regeneration, or IN droplet scavenging were considered in the model.

[16] There are some disadvantages to using a cloud-resolving model (CRM) framework to examine mixed phase microphysical sensitivities. Two of the most important are the following: The large horizontal grid spacing precludes examining cloud dynamical feedbacks associated with liquid and ice crystal growth [e.g., *Korolev and Field*, 2008; *Korolev*, 2007]. In addition, the CRM can only marginally resolve boundary layer eddies. The eddies that are resolved are 2-D mesoscale eddies, and it cannot be argued that these are completely realistic since no coastline or other features exist in the CRM. Moreover, alternative nucleation mechanisms like those discussed by *Fridlind et al.* [2007] cannot be included since they depend on the evaporation of drops in downdrafts, which are not resolved in a CRM. In order to include evaporation IN and evaporation freezing, updrafts and downdrafts within the cloud should be predicted. Both mechanisms require the evaporation of drops, which are spatially correlated with the downdrafts. Hence, we expect that there should be a strong relationship between some nucleation mechanisms and updraft/downdraft structure. However, since the CRM cannot resolve the updrafts and downdrafts, the structural correlation cannot be captured. These disadvantages should be borne in mind throughout our discussion.

[17] To investigate the influence of parameterized habit on mixed phase cloud simulations, we performed a series of sensitivity studies using different crystal shapes. This study was motivated in part by prior simulations that produced faster glaciation [*Harrington et al.*, 1999; *Prenni et al.*, 2007] as compared to other studies using similar IN concentrations [e.g., *Fridlind et al.*, 2007; *Morrison et al.*, 2008]. Three crystal shapes were used in the simulations: hexagonal plates, dendrites, and spheres. Dendrites and hexagonal plates were chosen because many models assume plate-like crystals in the temperature and supersaturation ranges for the clouds we simulated (-11°C to -16°C). Spherical shapes were included in part because they are the most compact "crystal" for a given size and have the largest fall speed. Consequently, spheres provide the greatest contrast to dendrites, which have the largest growth rate, but the smallest fall speed for a given size. In addition, including spheres in our simulations allows us to compare our results to studies that used a spherical shape [*Fridlind et al.*, 2007; *Morrison et al.*, 2008]. Our habit choices, as we discuss in section 6, cover the range from the fastest growing crystals but slowest falling (dendrites) to the slowest growing crystals but fastest falling (spheres). These shapes were chosen even though observations indicate the existence of a fair number of columns, irregular polycrystals, and spheres [e.g., *McFarquhar et al.*, 2007]. However, our purpose is to indicate the range of possible sensitivities produced by standard model habit assumptions and to resolve discrepancies between our modeling studies of these cases [e.g., *Prenni et al.*, 2007; *Klein et al.*, 2009; *Morrison et al.*, 2009] and those of other authors [e.g., *Fridlind et al.*, 2007; *Morrison et al.*, 2008].

[18] The mass and fall speed relationships reported in the literature for ice span a relatively large range for a given size [*Pruppacher and Klett*, 1997; *Mitchell*, 1996; *Heymsfield and Kajikawa*, 1987; *Heymsfield et al.*, 2002]. Hence, we examine the sensitivity of model-simulated mixed phase clouds to the span in these relations, which are shown as the gray areas in Figures 2a and 2b. For our simulations, we

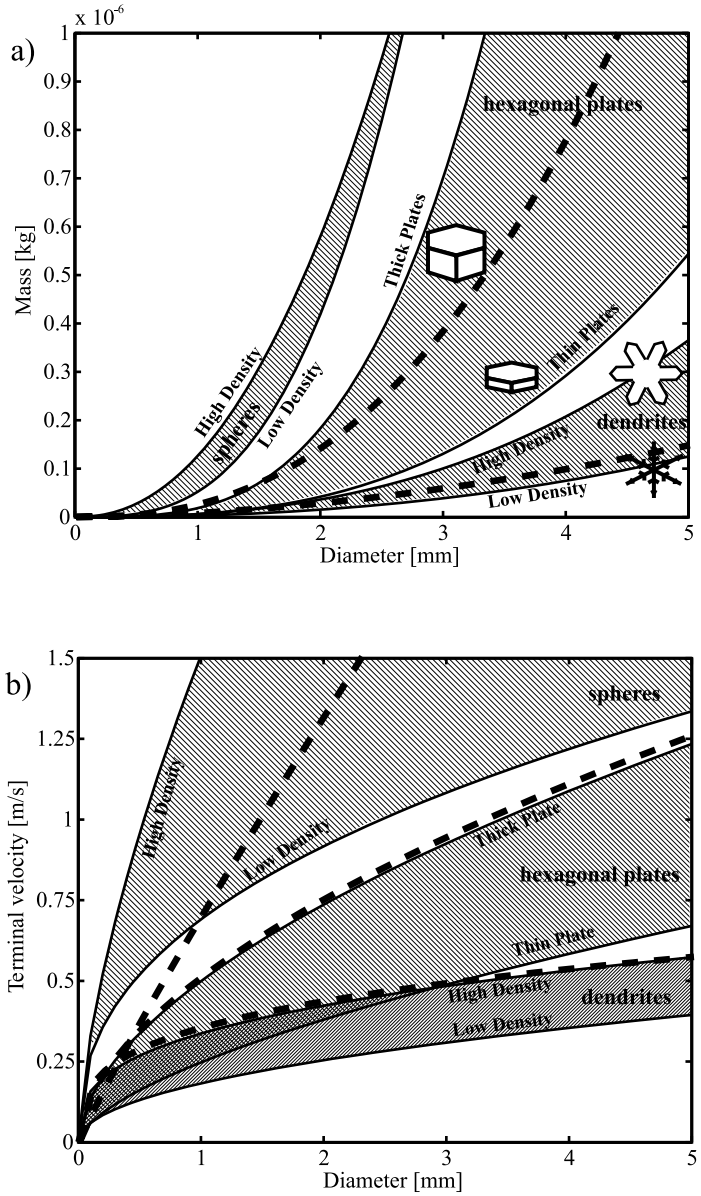

Figure 2. Ranges of (a) mass-dimensional and (b) fall speed relations of the crystal habits used in the simulations. The extremes of the range for each habit are defined by the highest-density and lowest-density particles for spheres and dendrites and by the thickest and thinnest plates for hexagonal plates. The terms "high density" or "thick plate" and "low density" or "thin plate" are used to refer to the extremes for each range. Mass-dimensional and fall speed relations used in "control" runs are shown with broken lines.

select relations that define the maximum and minimum, or the extremes, for each mass and fall speed range. These relations are applied to both pristine ice and snow categories in the model. The sensitivity of the simulated cloud with respect to crystal habit is then investigated using these extremes. Physically, the extremes of each range refer to the density, or the compactness, of the crystal: The curves that define the upper range of the mass and fall speed relations are associated with high-density crystals in the case of spheres and dendrites (broad-branched stellars) and thick plates in the case of hexagonal crystals. Similarly, the curves defining the lower range are associated with low-density crystals in the case of spheres and dendrites (classic dendrites) and thin plates in the case of hexagonal crystals. These terms for the extremes will be used throughout the paper. The coefficients in mass-dimensional and fall speed relations for these extremes are presented in Table 1. For spheres, we used relations similar to those of *Fridlind et al.* [2007] and *Morrison et al.* [2008].

[19] How compact, or dense, a crystal is has important consequences for vapor growth. For the same volume, more compact, dense crystals have weaker vapor growth rates [e.g., *Chen and Lamb*, 1994; *Fukuta and Takahashi*, 1999; *Sheridan et al.*, 2009]. To illustrate this dependence, the growth of an equivalent volume sphere is compared to predictions from the adaptive habit model of *Chen and Lamb*

Table 1. Coefficients in Mass-Dimensional and Fall Speed Relations and Shape Factor for Ice Crystal Habits Used in the Simulations

Habit	α_m	β_m	α_{vt}	β_{vt}	S
Dendrites					
High density	0.2423	2.53	3.29	0.33	0.31
Low density	0.0233	2.29	5.02	0.48	0.31
Hexagonal plates					
Thick	156.74	3.31	24.37	0.56	0.31
Thin	1.43	2.79	17.90	0.62	0.31
Spheres					
High density	0.5020	2.20	143.9	0.66	0.5
Low density	52.36	3.00	11.72	0.41	0.5
Control dendrites	0.0020	1.80	2.81	0.30	0.31
Control hexagonal plates	0.5870	2.45	24.87	0.56	0.31
Control spheres	52.36	3.00	386.8	0.91	0.5

[1994]. The *Chen and Lamb* [1994] model was used because it accurately simulates the evolution of crystal mass and aspect ratio at water saturation. After 20 min of growth, the mass of an equivalent volume sphere is significantly smaller than the accurate model except at the transition temperatures between habits (approximately $-9°C$ and $-20°C$) where habit growth is roughly isometric (Figure 3). The upper edge of the mass range (gray-shaded area) in the plates regime used the RAMS standard formulation for dendrites, whereas the lower range used a thick hexagonal plate. Consequently, we should expect more isometric, and compact, crystals to grow more slowly in time leading to a weaker Bergeron process.

[20] The shape factor (S) in the crystal capacitance (equation (3)) has a different value for each habit and is held constant during a simulation even though S varies with aspect ratio [e.g., *Westbrook et al.*, 2008]. While analytical forms of S for spheres and spheroids exist [*Chen and Lamb*, 1994], S for dendrites and hexagonal shapes must be computed numerically [*Westbrook et al.*, 2008]. Because vapor growth depends on S, we include a series of simulations in which S is varied.

5. Baseline Simulations and Comparison With Observations

[21] Our baseline simulations for the single-layer and multilayer cases examine the combinations of physical factors (IN concentration and habit) necessary to produce the best overall comparison with data taken during M-PACE. We undertake these studies precisely because of the large range of mass and fall speed relations available (Figure 2). Furthermore, the baseline results provide a framework for discussions of the sensitivities to habit parameterization.

5.1. Single-Layer Cloud: Case B

[22] The observed LWP data are derived from microwave radiometer measurements [*Turner et al.*, 2007] and are averaged for the three sites: Atqasuk, Barrow, and Oliktok. The uncertainty in the retrieved LWP data was estimated to be 20 g m^{-2} [*Turner et al.*, 2007; *Klein et al.*, 2009]. For ice water path (IWP), we used the estimated IWP range from *Klein et al.* [2009]. The best match between the simulations and the observed LWP and IWP was obtained with high-density dendrites (stellars) and M-PACE IN concentrations (Figures 4a and 4b).

[23] The simulation with high-density dendrites produces LWP oscillations that follow the observations remarkably well and range between 90 and 170 g m^{-2} (Figure 4a). An analysis of the simulation (not shown) suggests that the lag correlation between the LWP and IWP peaks (Figure 4b) is caused by the entrainment of IN-rich air from above the cloud, producing ice precipitation and a decrease of the LWP similar to *Carrio et al.* [2005]. The IN depletion by ice sedimentation allows for a consequent LWP increase similar to *Harrington and Olsson* [2001] though the simulated IWP is below the estimated IWP except during the precipitation periods (Figure 4b). It should be pointed out, however, that the entrainment is not explicitly resolved in the CRM framework.

[24] The simulated liquid water content (LWC) and IWC profiles are compared to aircraft observations in Figures 5a and 5b. Measurement data from flight 10a [*McFarquhar et al.*, 2007] and modeled quantities are averaged over the flight duration; modeled quantities are also averaged over the domain. The uncertainties in LWC measurements are ±15% [*McFarquhar et al.*, 2007] and a factor of 2 for the IWC in ice-only regions [*Klein et al.*, 2009]. The simulated LWC is lower than the observations in the lower half of the cloud layer, but the match is better near cloud top (Figure 5a).

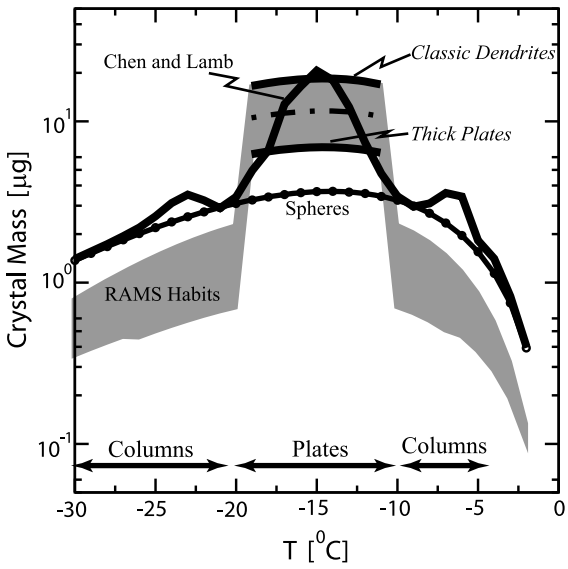

Figure 3. Crystal mass as a function of temperature for a single particle grown for 20 min at water saturation. The solid line is from the *Chen and Lamb* [1994] spheroid approximation to crystal growth, which is considered to be relatively accurate at water saturation. The solid line with circles is for equivalent volume spheres using the reduced density from *Chen and Lamb* [1994, equation (42)]. The gray areas indicate the range of masses predicted using the standard RAMS mass and capacitance. In the plate regime, RAMS low-density (classic) dendrites define the upper edge of the gray area, whereas the lower edge is defined by thick plates. The dash-dotted line is for thin plates and high-density (stellar) dendrites, which have very similar model growth rates.

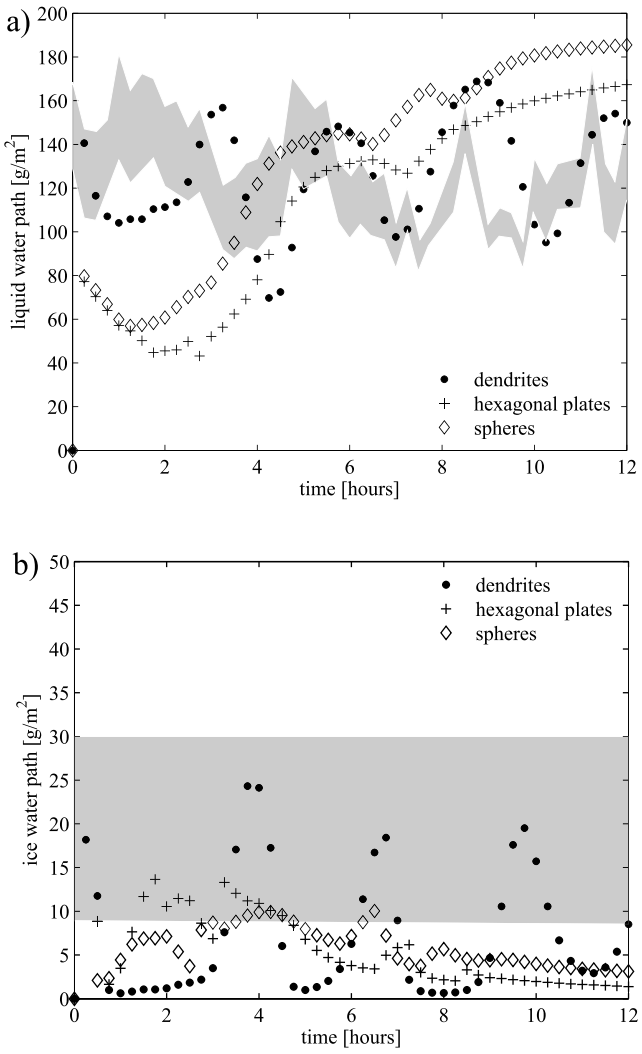

Figure 4. Time series of simulated (symbols) and retrieved (shaded) (a) liquid and (b) IWP (g m^{-2}) for the single-layer case. Simulated quantities are domain averaged. Shaded area in Figure 4a represents the 95% confidence interval of observational data and IWP range in Figure 4b is an estimate from *Klein et al.* [2009].

The predicted IWC, however, is underestimated by about a factor of 2 inside the liquid layer and a factor of 10 below cloud base (Figure 5b). The low IWCs are due primarily to the depletion of IN by nucleation scavenging, which also leads to very low ice concentrations [cf. *Harrington and Olsson*, 2001; *Fridlind et al.*, 2007]. Although the simulation compares well with the observed LWP, this is somewhat fortuitous as the results depend on the mass and fall speed relations (see section 6).

[25] In addition to the simulations with high-density dendrites, we performed two simulations using spheres and thick plates. Both simulations produced a liquid cloud layer with essentially no ice when the M-PACE IN concentrations were used (not shown). The only way the simulated LWP and IWP could be brought into closer agreement with the observations was by increasing the M-PACE IN concentration by a factor of 25. Thick plates and spheres, which grow more slowly than the dendrites but fall faster, require higher IN concentrations to produce a similar match with observations (Figures 4a and 4b). We note that using this larger IN concentration in simulations with high-density dendrites led to the glaciation of the cloud layer, similar to prior results using RAMS [*Harrington and Olsson*, 2001; *Prenni et al.*, 2007]. It is apparent that mixed phase cloud sensitivity to IN concentrations depends on the assumed ice habit.

[26] Although both the LWP and IWP are similar for all three crystal habits, the time evolution shows that there are considerable differences. Only the simulation using high-density dendrites adequately captured the oscillations in the observed LWP. The slower vapor growth and greater fall speeds of hexagonal and spherical ice lead to a different temporal evolution of the LWP and IWP. Even though the simulations with spheres and plates have a higher ice concentration (not shown), the IWP and IWC are still well below the observed range (Figures 4 and 5). The simulated

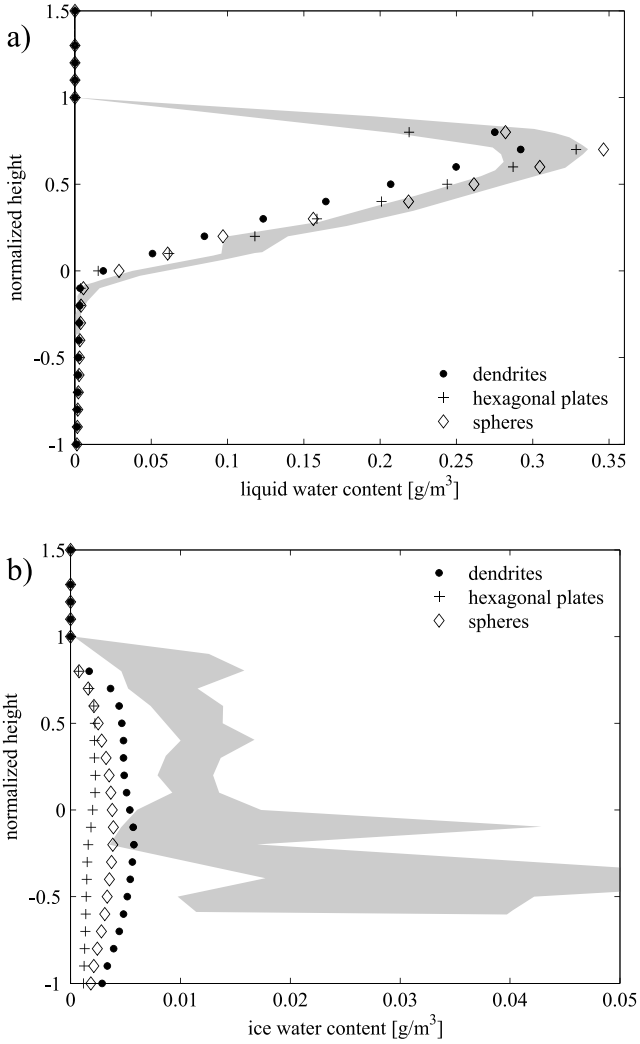

Figure 5. Time-averaged vertical profiles of simulated domain-averaged (symbols) and observed (shaded) (a) liquid and (b) IWC (g m^{-3}) for the single-layer case. Simulated and observed quantities are averaged over the flight duration. Shaded area represents the 95% confidence interval of observational data.

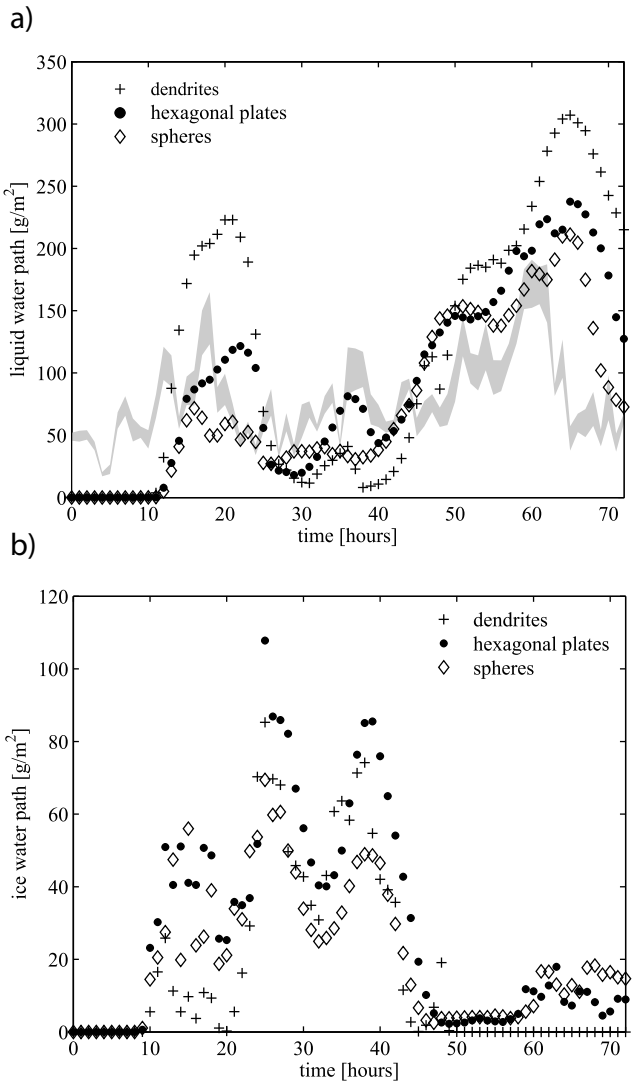

Figure 6. Time series of simulated (symbols) and retrieved (shaded) (a) liquid and (b) IWP (g m^{-2}) for the multilayer case. Simulated quantities are domain averaged. The shaded area in Figure 6a represents the 95% confidence interval of observational data.

ice concentration for all three cases was 1–3 orders of magnitude lower than observations, similar to the simulations of *Morrison et al.* [2005] and *Fridlind et al.* [2007]. This underprediction of ice concentrations and ice mass is a perennial modeling problem that has been addressed, for this case, by *Fridlind et al.* [2007].

5.2. Multilayered Cloud: Case A

[27] Similar to the single-layer case, the simulations for each habit were compared with the ground-based LWP retrievals of *Turner et al.* [2007] and airborne measurements (data from Department of Energy–Atmospheric Radiation Measurement (DOE-ARM) archive) as shown in Figures 6 and 7. No clouds were produced by any simulation for the first 10 h (Figure 6). The simulation with high-density dendrites used M-PACE IN concentrations and overestimated the peaks in the LWP during the first and final 24 h and underestimated the LWP in the middle of the simulation. As in the single-layer case, IN concentrations were increased by 25 times the M-PACE values so that spheres and thick plates could be brought into better agreement with the observations. The best correspondence with observations was achieved using thick plates where simulated LWP followed the observations reasonably well. Comparisons of our results with those of *Morrison et al.* [2009, Figure 9] reveal that our IWP values were, on average, 2 times lower than the retrieved IWP. Vertical profiles of LWC and IWC observed during the 6 October flight (DOE-ARM data archive) and simulated profiles, averaged for the duration of the flight, are presented in Figure 7. The maxima in the aircraft-derived LWC (Figure 7a) and radar observations (J. Verlinde, personal communication, 2008) indicate the presence of four to five liquid layers. At the time of the aircraft observations, the simulation with spheres produced only one liquid layer around 1000 m. Two layers were produced in the simulations with

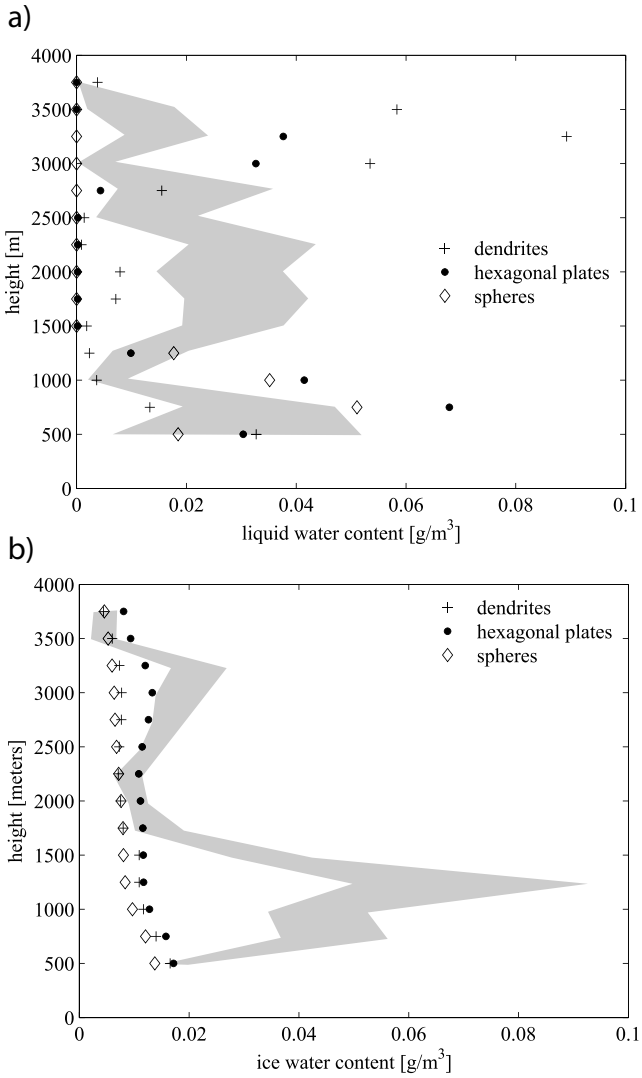

Figure 7. Time-averaged vertical profiles of simulated, domain-averaged (symbols), and observed (shaded) (a) liquid and (b) IWC (g m^{-3}) for the multilayer case. Simulated and observed quantities are averaged over the flight duration. Shaded area represents the 95% confidence interval of observational data.

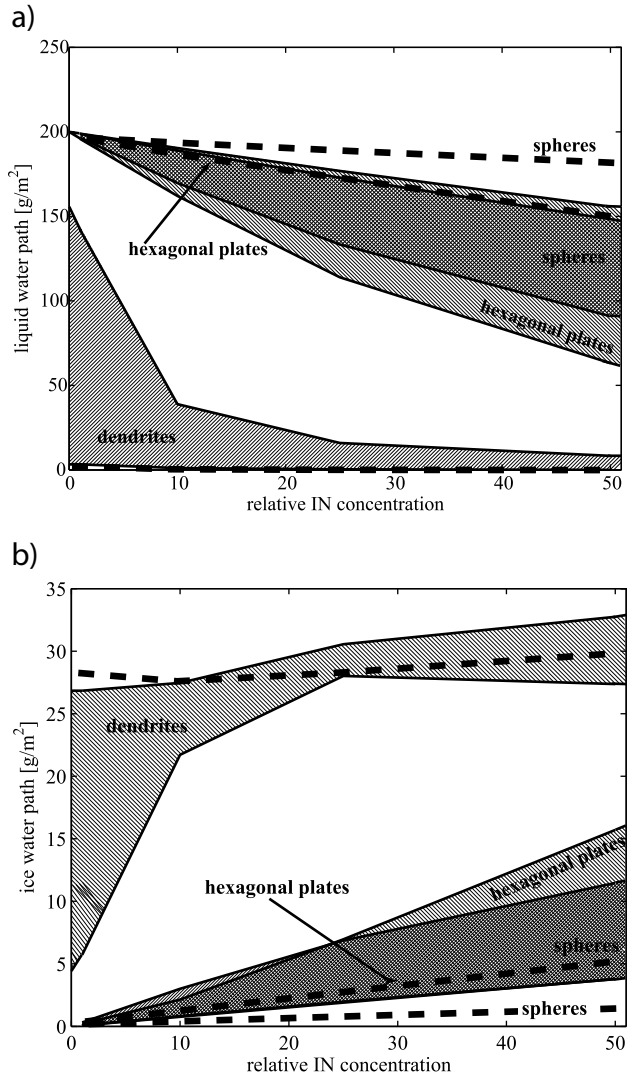

Figure 8. Ranges of simulated (a) liquid and (b) IWP (g m^{-2}) for different habits as a function of IN concentration for the single-layer case. "Control" runs are shown with broken lines. Simulated quantities are domain and simulation averaged. IN concentration is relative to 0.15 L^{-1}.

thick plates with one around 1000 m and the second at about 3000 m, though the LWC of both layers is overestimated. In addition to these two layers, the simulation with high-density dendrites produced a third layer at about 2000 m. This contrasts with the observations (Figure 7a), which show two separate layers near 2000 m (2250 and 1750 m) and 3000 m (3250 and 2750 m). Given the coarse vertical grid spacing at these heights (90–100 m) it is possible that the model is underresolving the layers. Regardless, the LWC of the top layer is overestimated. All three simulations underestimate the IWC (Figure 7b), especially between 1500 and 500 m, while above 1500 m the simulation with thick plates produces a better match with the observations.

6. Sensitivity to Parameterized Habit

[28] The above results show that the IN concentration sensitivity and the number of liquid layers depend on the assumed ice habit. Furthermore, prior studies using high-density dendrites [*Prenni et al.*, 2007] show a stronger sensitivity to IN concentration than studies that used spheres [e.g., *Fridlind et al.*, 2007; *Morrison et al.*, 2008]. These factors motivated us to examine the influence of the choice of habit (mass and fall speed relations and capacitance) on phase partitioning between liquid and ice in mixed phase clouds. To explore the model sensitivity to parameterized habit, sensitivity simulations for each habit were done using all four possible combinations of the extremes in the mass and fall speed relations (Figure 2). The IN concentration was also varied from the M-PACE value ($\sim$0.15 L^{-1}, defined as a relative IN concentration of 1) to a value 50 times larger (defined as a relative IN concentration of 50). We should point out that the use of empirically derived mass-dimensional and fall speed relations that are not connected through the Best number, as discussed by *Mitchell* [1996], can potentially lead to physical inconsistencies in model simulations. To make certain that our use of such relations does not have a significant impact on the qualitative nature of our results, another three "control" series of simulations (one for each habit) were conducted. In these series, we used coefficients in fall speed relation calculated following *Mitchell* [1996]. To calculate these coefficients, we used mass-dimensional and area-dimensional data [*Mitchell*, 1996, Table 1] for hexagonal plates and broad-branched dendrites. For spheres, we used the mass-dimensional relation given by *Morrison et al.* [2008], assuming perfect spherical shape for the area-dimensional relation. In calculating all coefficients in fall speed relation the appropriate size, Reynolds and Best number ranges were taken into account. The mass-dimensional and fall speed relations for "control" runs are shown in Figure 2, and the coefficients are listed at the end of Table 1. We begin by discussing sensitivities to mass and fall speed relations.

6.1. Mass and Fall Speed Sensitivities

[29] To illustrate the overall influence of mass and fall speed choice on simulated phase partitioning, we computed simulation-averaged LWP and IWP for all IN concentrations and for each sensitivity simulation. The range of possible LWP and IWP produced by using the four combinations of mass and fall speed relations for each habit, as well as results of "control" runs, are shown in Figure 8 for the single-layer case.

[30] Simulations with hexagonal plates and spheres produced similar results (Figure 8) though with a different spread: The LWP was greatest and the IWP was smallest for these habits. At low IN concentrations the LWP and IWP do not show much sensitivity to the mass and fall speed relations associated with hexagonal plates and spheres. As the IN concentration increases, the spread of LWP and IWP variation also increases, reaching relative differences of up to 60% and 75%, respectively. The respective upper and lower bounds of the LWP range are defined by simulations with high-density or thick (slow vapor growth, fast falling) and low-density or thin (fast vapor growth, slow falling) crystals. Simulations using thick plates or high-density spheres produced the largest LWP and smallest IWP, whereas the converse is true for low-density spheres and thin plates. Physically, this makes sense because more compact, isometric particles have lower vapor growth rates at our cloud temperature (approximately -15°C; see Figure 3) but greater

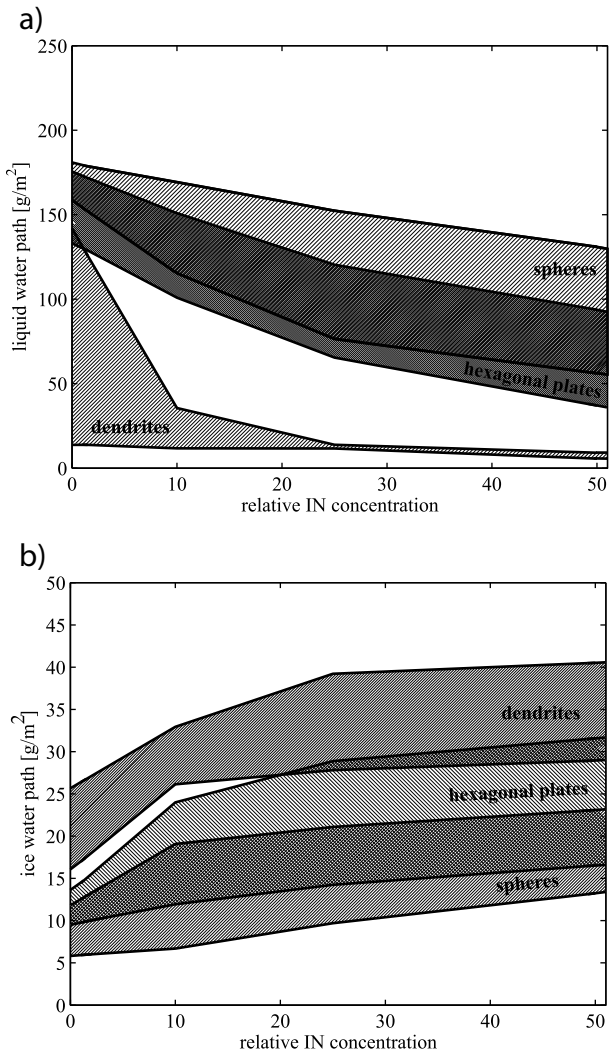

Figure 9. Ranges of simulated (a) liquid and (b) IWP (g m^{-2}) for different habits as a function of IN concentration for the multilayer case. Simulated quantities are domain and simulation averaged. IN concentration is relative to 0.15 L^{-1}.

fall speeds [e.g., *Fukuta and Takahasi*, 1999]. As Figure 3 shows, both thick and thin plates in RAMS have growth rates that are lower than those computed with an accurate ice crystal growth model. Spheres tend to define the upper limit in Figure 8a: They are the fastest falling particles with the slowest vapor growth rates (Figure 3), and consequently, more liquid can be maintained. The large difference in vapor growth rates and fall speeds for each habit is also the reason for the different IN sensitivity for each habit: The change in LWP with a relative IN increase from 1 to 50 for thin plates is 68% as compared to only 22% in the case of the thick plates.

[31] In contrast to simulations with hexagonal plates and spheres, simulations with dendrites show a stronger IN sensitivity. At low IN concentrations (<1 L^{-1}) simulations with high-density dendrites produced a LWP and IWP that are closer to the simulations with spheres and hexagonal plates (upper curve on the dendrite range in Figure 8a). Increasing the IN concentration leads to a larger reduction in the LWP as compared to spheres or hexagonal plates and is similar to prior studies with dendrites [*Harrington and Olsson*, 2001; *Jiang et al.*, 2000; *Prenni et al.*, 2007]. In the case of low-density (classic) dendrites, the LWP is negligible even at low IN concentrations (lower curve on the dendrite range in Figure 8a). The large range of sensitivity for dendrites makes physical sense. Dendrites have the largest vapor growth rates, but the lowest fall speed, of any habit. The rapid dendrite growth is clearly indicated in Figure 3 by the *Chen and Lamb* [1994] result at −15°C. In addition, the mass relation used in RAMS for dendrites and plates leads to a significant range of possible crystal growth rates (shaded region, Figure 3). Thus, it should be expected that a large sensitivity to changes in the mass relationship, and a wide range of possible LWP and IWP (Figure 8), would exist. The water path ranges are greatest at low IN concentrations for dendrites because crystal sizes are the largest here, leading to the strongest vapor growth, the largest liquid depletion rates, and hence the largest sensitivity to the mass relations.

[32] Results from "control" simulations showed a similar behavior, confirming the validity of simulations discussed above. The greatest LWP and smallest IWP were obtained for spheres and hexagonal plates. The sensitivity to IN concentration is also similar to that of their "empirical counterparts." Simulations with "control" dendrites produced a LWP and IWP that are very close to those produced by low-density dendrites.

[33] Analogous sensitivities to mass and fall speed parameterizations were obtained for the multilayer cases, which are shown in Figure 9. Simulations with hexagonal plates and spheres again produced the highest LWP for a given IN concentration, whereas dendrites produced the lowest. As in the single-layer case, the high-density crystals and thick plates produced the greatest LWP as compared to low-density crystals and thin plates. The low-density dendrites are associated with a very low LWP, whereas the high-density dendrites produce a higher LWP and have a high sensitivity to IN concentration.

[34] Figures 8 and 9 indicate that both the single-layer and multilayer clouds have a similar response to parameterized habits, though with some interesting differences. First of all, note that the maximum possible LWP in the single-layer case is the same for both thick plates and spheres (the top curves defining the shaded regions in Figure 8a). In contrast, the maximum LWP in the multilayer cloud simulations occurs when spheres are used (Figure 9a). The reason for this difference has to do with the larger vertical extent of the multilayer cloud system. In the single-layer case, spheres and thick plates fall fast enough (Figure 2b) such that they are removed from the liquid layer before they can deplete significant amounts of liquid. However, in the multilayer case liquid water is depleted by crystals nucleated within each layer and by larger crystals that fall into the layer from above (the seeder-feeder process). In this case, the fall speed difference between hexagonal plates and spheres is crucial as the spherical crystals fall more rapidly through the lower cloud layers therefore depleting less liquid (Figure 9a). This is also the reason for the greater sensitivity to the mass and fall speed relations for spheres and hexagonal plates at low IN concentrations as compared to the single-layer case (Figures 8a and 9a).

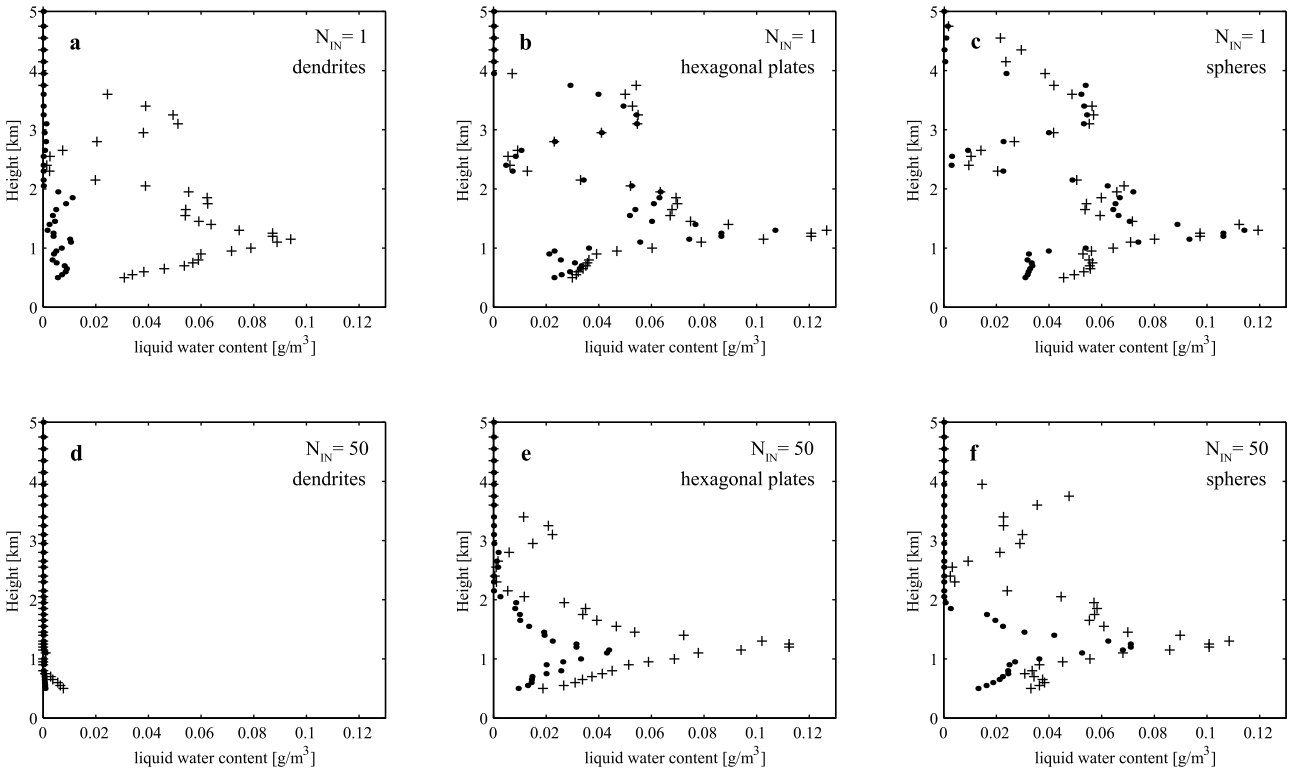

Figure 10. Simulation-averaged and domain-averaged vertical profiles of liquid water content (g m^{-3}) for different habits at relative IN concentration of (a–c) 1 and (d–f) 50. Simulations were conducted for all four combinations of mass and fall speed relations. Only the simulations that produced the highest (crosses) and the lowest (dots) liquid water path are shown here.

6.2. Multiple-Layering Dependence on Habit

[35] As was shown in section 5, the number of liquid layers depends on habit (Figure 6a). Examining this issue in detail is beyond the scope of this article, but information can be gained by examining the differences in the cloud vertical structure produced by the different habit parameterizations. Figure 10 shows simulation-averaged LWCs for the three habits at relative IN concentrations of 1 and 50. We should note, however, that averaging over such a long period of time cannot completely illustrate the multilayered structure of simulated clouds. We show only the sensitivity simulations that produced the highest and lowest LWPs for each habit. The number of liquid layers in the simulations varies from one (high-density dendrites at $N_{IN} = 50$) to five (spheres at $N_{IN} = 1$). In general, simulations with high-density dendrites produced fewer liquid layers (one to three) than simulations with spheres (one to five layers) or thick plates (one to four layers). The influence of IN concentration on the number of layers is stronger for the faster growing, slower falling dendrites. When N_{IN} is increased from 1 to 50, the simulation with dendrites produces one marginal liquid layer, whereas hexagonal plates and spheres produce from one to five layers. The greater sensitivity to IN concentration and the fewer number of layers for the dendrite simulation can be explained using our prior results: Dendrites have the largest growth rates (Figure 3) and the lowest fall speeds (Figure 2); consequently, the seeder-feeder process operates more efficiently and so the liquid layers are quickly depleted. This is the primary reason for the loss of all liquid cloud layers when N_{IN} is increased from 1 to 50 in the dendrite case. Since spheres have the weakest growth rates, and the largest fall speeds, the number of liquid layers and the LWP are much less sensitive to an increase in N_{IN}. Simulations with hexagonal plates tend to fall in between the simulations with dendrites and spheres.

6.3. Analysis of Mass, Fall Speed, and Capacitance Effects

[36] The simulations presented above illustrate that the liquid and ice in mixed phase clouds depend not only on the IN concentration but also on the assumed habit and the way that habit is parameterized. However, the above results do not allow us to separate the relative importance of the mass, fall speed, and capacitance relationships. As a consequence, we performed another series of simulations in which two of the relationships that define the model habit are held fixed while the third is modified. We use high-density dendrites for our analysis given the strong model sensitivity to this habit and we discuss only the single-layer case.

[37] In order to determine the relative importance of the mass relation, we replaced the dendrite mass relation with that for thick plates (Figure 2a). Simulations were then done using the two dendrite fall speed relations that bound the shaded region in Figure 2b. The range of the model results from these simulations is shown as the gray-shaded region for "plate mass" in Figure 11. By changing the mass relation to that of a thick plate, the vapor growth rate is reduced (Figure 3) and so the LWP increases (Figure 11). At low IN

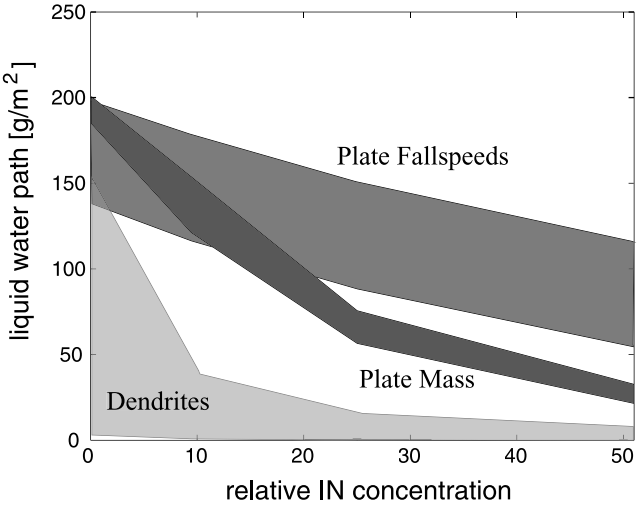

Figure 11. Range of domain-averaged and simulation-averaged LWP for the following simulations: Dendrites indicate the range of LWP as given in Figure 8a. The plate mass range indicates simulations in which the mass relation for a thick hexagonal plate is used in combination with the largest, and smallest, fall speed relations for dendrites. The plate fall speed range indicates simulations in which the thick plate fall speed relation is used in combination with the extremes in the dendrite mass relation. The IN concentration is relative to 0.15 L^{-1}.

concentrations, the LWP increased from the dendrite range (Figure 11) to nearly the values for hexagonal plates and spheres (Figure 8a). Note that the sensitivity to IN concentration is reduced when the vapor growth rate decreases but is still larger than the simulations with hexagonal plates and spheres (compare Figures 11 and 8a) because the fall speed of dendrites is low.

[38] We next examine the influence of fall speed by using the relation for thick plates (Figure 2b) in place of the relation for dendrites, which effectively removes the dendrites more quickly from the liquid layer. Simulations were then done for the mass relations of high-density and low-density dendrites (Figure 2a). The ranges of the simulation results for "plate fall speeds" are shown in Figure 11. The greater fall speed causes the LWP of the dendrite simulations to increase and the IN sensitivity to decrease significantly. This result indicates that the weaker IN sensitivity in the hexagonal plate and sphere simulations is likely due to the large fall speeds. Note that the range of LWP is still relatively large because the different mass relations lead to different vapor growth rates (Figure 3).

[39] As discussed in section 3, the shape factor (S) in the capacitance (equation (3)) is held constant in RAMS even though it varies with aspect ratio [*Westbrook et al.*, 2008]. To examine the impact of fixing S, simulations were conducted where S was varied from 0.31 down to 0.22, covering a realistic range of S [see *Westbrook et al.*, 2008, Figure 11; *Sheridan et al.*, 2009]. Simulation results are shown in Figure 12. For low-density dendrites, varying S has a small impact on the simulated LWP. The low density for a given size (Figure 2a) produces large vapor growth rates (Figure 3, classic dendrites at -15°C), and coupled with low fall speeds (Figure 2b) produces rapid depletion of the liquid regardless of the value of S. For the high-density dendrites, however, the impact of S on the LWP is significant. The higher density for a given size produces weaker growth rates (Figure 3, at -15°C), and so changes in S become important. Although the sensitivity to IN concentration remains high, decreasing S leads to reduced vapor growth rates (equation (3)) and to a considerable increase in the LWP.

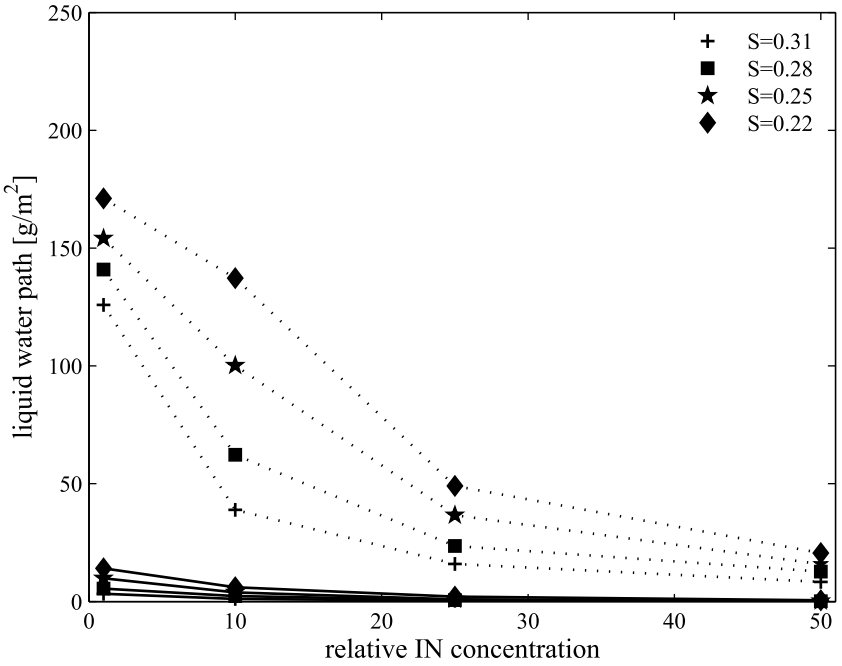

Figure 12. Domain-averaged and simulation-averaged LWP for low-density (solid line) and high-density (dotted line) dendrites as a function of IN concentration. The IN concentration is relative to 0.15 L^{-1}.

[40] It should be noted that this sensitivity to S is somewhat artificial. In reality, S should change in time as the aspect ratio of the crystal changes [*Chen and Lamb*, 1994]. The impact of fixing S can be readily discerned in Figure 3: Note that the RAMS model produces growth rates lower than those for spheres over the ranges of columnar growth. This is unrealistic and is due to the use of thick hexagonal columns (aspect ratios <10) that have a low growth rate and, coupled with a fixed S, leads to a capacitance that is too small. These results suggest that parameterizing the shape factor can be as important as the mass relations used in a model.

7. Summary and Concluding Remarks

[41] Many models parameterize crystal habit by using equations that relate mass and fall speed to the maximum dimension of the crystal. Cloud-resolving model simulations of single-layer and multilayer mixed phase clouds observed during the M-PACE were undertaken in order to examine the importance of parameterized habit to mixed phase cloud evolution. Mass, fall speed, and shape relations from the literature were used for hexagonal plates, dendrites, and spheres for two reasons: First, the observed temperature range for M-PACE would cause most models to use a primary habit of a plate-like crystal. Second, simulations of the M-PACE cases by other models have used equivalent volume spheres with a reduced density.

[42] Our simulations suggest that the phase partitioning between liquid and ice depends on the mass and fall speed relation used in the model. For single-layer clouds, the best match with observed liquid and ice water paths (LWP and IWP, respectively) was produced by simulations with dendrites only when ambient IN concentrations were near the low-observed values ($\sim$0.15 L^{-1}). However, simulations with hexagonal plates and spheres could only be brought into better agreement with the observed LWP and IWP at higher IN concentrations. In contrast, for multilayer clouds, assuming thick hexagonal plate crystals with high IN concentrations produced the best match with observations. These results, however, are in contrast with in situ observations of ice crystal shapes during M-PACE case days [*Zhang et al.*, 2006; *McFarquhar et al.*, 2007]. While in both cases ice crystals smaller than 100 μm were predominantly spherical, the larger ice crystals in the multilayer case were more or less evenly distributed between needles, columns, spheres, and irregular shapes. In the single-layer case, although the percentage of irregular ice crystals was highest, there were also a significant number of bullet rosettes, needles, columns, and spherical shapes. It should be pointed out that these shapes were identified using an automated classification scheme that does not include dendrites.

[43] Our results suggest a different model response to ice nucleation depending on habit: Dendrites produce clouds with a strong sensitivity to IN concentrations, and probably ice nucleation in general, whereas simulations with hexagonal plates and spheres have a much weaker sensitivity to IN concentrations. The differing IN sensitivities are due to the different mass and fall speed relations. Compact crystals like thick hexagonal plates and spheres have weak vapor growth rates and large fall speeds whereas dendrites have large vapor growth rates and small fall speeds. Consequently, plates and spheres glaciate simulated mixed phase clouds slowly and therefore liquid can be maintained at higher ice concentrations than when fast growing habits like dendrites are assumed. Parameterized habit and IN concentration also have an influence on the number of multiple layers predicted by the model: Compact habits like plates and spheres support the existence of more cloud layers at all IN concentrations because the crystals grow more slowly and fall faster, which weakens the seeder-feeder process.

[44] The range of LWP and IWP simulated by the model depends on the mass and fall speed relation chosen from the literature. The range of possible mass and fall speed relations is relatively large. While the relation chosen does not affect the qualitative sensitivity of the simulated mixed phase cloud to IN concentrations for a given habit, it does impact the partitioning between LWP and IWP. For instance, dendrites show a strong sensitivity to IN concentration regardless of the mass and fall speed relation chosen; however, the range of possible LWP and IWP for this habit is relatively large. Sensitivity studies suggest that the mass and fall speed relations are of roughly equal importance in determining phase partitioning. In addition, fixing the shape factor in the capacitance has a significant impact on the simulated LWP and IWP.

[45] The results of our study suggest that any parameterization of habit should account for the link between mass, crystal geometry, and the capacitance. However, the feedback between evolving habits and vapor growth is not captured well by our model or by most other models [e.g., *Harrington et al.*, 1999; *Fridlind et al.*, 2007; *Morrison et al.*, 2008]. The recent model developed by *Hashino and Tripoli* [2007] does attempt to parameterize the influence of changing habit.

[46] Finally, our results also provide an interpretation for some conflicting results that exist in the literature. The mixed phase simulations of *Harrington et al.* [1999], *Jiang et al.* [2000], *Harrington and Olsson* [2001], and *Prenni et al.* [2007] show that the LWP in mixed phase clouds is strongly dependent on the IN concentration. These studies used dendrites, which were chosen by the model on the basis of the temperature. In contrast, the simulations by *Morrison et al.* [2005, 2008] and *Fridlind et al.* [2007] are much less sensitive to IN concentration and these studies used spheres. Our simulations suggest that these conflicting results are primarily due to the mass and fall speed parameterizations used by each model.

[47] **Acknowledgments.** The authors are grateful for support by the Office of Biological and Environmental Research of the U.S. Department of Energy (DE-FG02-05ER64058) as part of the Atmospheric Radiation Measurement Program. One of us (J. Y. Harrington) was also supported through a National Science Foundation grant (ATM-0639542). We are indebted to Dennis Lamb for insightful conversations regarding the growth of ice. Discussions of ice crystal growth and habits with Zachary Lebo, Kara Sulia, and Chengzhu Zhang helped to clarify many of the ideas presented in this work.

References

Avramov, A., and J. Y. Harrington (2006), The influence of ice nucleation mode and ice vapor growth on simulation of Arctic mixed-phase clouds, paper presented at 12th Conference on Cloud Physics, Am. Meteorol. Soc., Madison, Wis.

Bigg, E. K. (1996), Ice forming nuclei in the high Arctic, *Tellus, Ser. B*, *48*, 223–233.

Carrió, G. G., H. Jiang, and W. R. Cotton (2005), Impact of aerosol intrusions on Arctic boundary layer clouds. Part I: 4 May 1998 case, *J. Atmos. Sci.*, *62*, 3082–3093.

Chen, J. P., and D. Lamb (1994), The theoretical basis for the parameterization of ice crystal habits: Growth by vapor deposition, *J. Atmos. Sci.*, *51*, 1206–1222.

Cotton, R. J., and P. R. Field (2002), Ice nucleation characteristics of an isolated wave cloud, *Q. J. R. Meteorol. Soc.*, *128*, 2417–2437.

Cotton, W. R., M. A. Stephens, T. Nehrkorn, and G. J. Tripoli (1982), The Colorado State University three-dimensional cloud/mesoscale model—1982. Part II: An ice phase parameterization, *J. Rech. Atmos.*, *16*, 295–320.

Cotton, W. R., et al. (2003), RAMS 2001: Current status and future directions, *Meteorol. Atmos. Phys.*, *82*, 5–29.

Curry, J. A., and A. H. Lynch (2002), Comparing Arctic regional climate models, *Eos Trans. AGU*, *83*, 87.

Curry, J., W. Rossow, D. Randall, and J. Schramm (1996), Overview of Arctic cloud and radiation characteristics, *J. Clim.*, *9*, 1731–1764.

Francis, J. A., E. Hunter, J. R. Keu, and X. Wang (2005), Clues to variability in Arctic minimum sea ice extent, *Geophys. Res. Lett.*, *32*, L21501, doi:10.1029/2005GL024376.

Fridlind, A. M., A. S. Ackerman, G. McFarquhar, G. Zhang, M. R. Poellot, P. J. DeMott, A. J. Prenni, and A. J. Heymsfield (2007), Ice properties of single-layer stratocumulus during the Mixed-Phase Arctic Cloud Experiment (M-PACE): 2. Model results, *J. Geophys. Res.*, *112*, D24202, doi:10.1029/2007JD008646.

Fukuta, N., and T. Takahashi (1999), The growth of atmospheric ice crystals: A summary of findings in vertical supercooled cloud tunnel studies, *J. Atmos. Sci.*, *56*, 1963–1979.

Harrington, J. Y., and P. Q. Olsson (2001), On the potential influence of ice nuclei on surface-forced marine stratocumulus cloud dynamics, *J. Geophys. Res.*, *106*, 27,473–27,484.

Harrington, J. Y., M. P. Meyers, R. L. Walko, and W. R. Cotton (1995), Parameterization of ice crystal conversion processes due to vapor deposition for mesoscale models using double-moment basis functions. Part I: Basic formulation and parcel model test, *J. Atmos. Sci.*, *52*, 4344–4366.

Harrington, J. Y., T. Reisin, W. R. Cotton, and S. M. Kreidenweis (1999), Cloud resolving simulations of Arctic stratus. Part II: Transition-season clouds, *Atmos. Res.*, *51*, 45–75.

Hashino, T., and G. J. Tripoli (2007), The Spectral Ice Habit Prediction System (SHIPS). Part I: Model description and simulation of the vapor deposition process, *J. Atmos. Sci.*, *64*, 2210–2237.

Heymsfield, A. J., and M. Kajikawa (1987), An improved approach to calculating terminal velocities of plate-like crystals and graupel, *J. Atmos. Sci.*, *44*, 1088–1099.

Heymsfield, A. J., A. Bansemer, S. Lewis, J. Iaquinta, M. Kajikawa, C. Twohy, M. R. Poellot, and L. M. Miloshevich (2002), A general approach for deriving the properties of cirrus and stratiform ice cloud particles, *J. Atmos. Sci.*, *59*, 3–29.

Hobbs, P. V., and A. L. Rangno (1998), Microstructure of low- and middle-level clouds over the Beaufort Sea, *Q. J. R. Meteorol. Soc.*, *124*, 2035–2071.

Intrieri, J. M., M. D. Shupe, T. Uttal, and B. J. McCarty (2002), An annual cycle of Arctic cloud characteristics observed by radar and lidar at SHEBA, *J. Geophys. Res.*, *107*(C10), 8030, doi:10.1029/2000JC000423.

Jiang, H., W. R. Cotton, J. O. Pinto, J. A. Curry, and M. J. Weissbluth (2000), Sensitivity of mixed-phase Arctic stratocumulus to ice forming nuclei and large-scale heat and moisture advection, *J. Atmos. Sci.*, *57*, 2105–2117.

Kay, J. E., T. L'Ecuyer, A. Gettelman, G. Stephens, and C. O'Dell (2008), The contribution of cloud and radiation anomalies to the 2007 Arctic sea ice extent minimum, *Geophys. Res. Lett.*, *35*, L08503, doi:10.1029/2008GL033451.

Klein, S. A., et al. (2009), Intercomparison of model simulations of mixed-phase clouds observed during the ARM Mixed-Phase Arctic Cloud Experiment. I: Single-layer cloud, *Q. J. R. Meteorol. Soc.*, *135*, 979–1002, doi:10.1002/qj.416.

Korolev, A. (2007), Limitations of the Wegener–Bergeron–Findeisen mechanism in the evolution of mixed-phase clouds, *J. Atmos. Sci.*, *64*, 3372–3375.

Korolev, A., and P. R. Field (2008), The effect of dynamics on mixed-phase clouds: Theoretical considerations, *J. Atmos. Sci.*, *65*, 66–86.

Korolev, A. V., and G. A. Isaac (2003), Phase transformation in mixed-phase clouds, *Q. J. R. Meteorol. Soc.*, *129*, 19–38.

McFarquhar, G. M., G. Zhang, M. R. Poellot, G. L. Kok, R. McCoy, T. Tooman, A. Fridlind, and A. J. Heymsfield (2007), Ice properties of single-layer stratocumulus during the Mixed-Phase Arctic Cloud Experiment: 1. Observations, *J. Geophys. Res.*, *112*, D24201, doi:10.1029/2007JD008633.

Meyers, M. P., P. J. Demott, and W. R. Cotton (1992), New primary ice-nucleation parameterizations in an explicit cloud model, *J. Appl. Meteorol.*, *31*, 708–721.

Meyers, M. P., R. L. Walko, J. Y. Harrington, and W. R. Cotton (1997), New RAMS cloud microphysics parameterization. Part 2: The two-moment scheme, *Atmos. Res.*, *45*, 3–39.

Mitchell, D. L. (1996), Use of mass- and area-dimensional power laws for determining precipitation particle terminal velocities, *J. Atmos. Sci.*, *53*, 1710–1723.

Morrison, H., M. D. Shupe, J. O. Pinto, and J. A. Curry (2005), Possible roles of ice nucleation mode and ice nuclei depletion in the extended lifetime of Arctic mixed-phase clouds, *Geophys. Res. Lett.*, *32*, L18801, doi:10.1029/2005GL023614.

Morrison, H., J. O. Pinto, J. A. Curry, and G. M. McFarquhar (2008), Sensitivity of modeled Arctic mixed-phase stratocumulus to cloud condensation and ice nuclei over regionally varying surface conditions, *J. Geophys. Res.*, *113*, D05203, doi:10.1029/2007JD008729.

Morrison, H., et al. (2009), Intercomparison of model simulations of mixed-phase clouds observed during the ARM Mixed-Phase Arctic Cloud Experiment. II: Multi-layered cloud, *Q. J. R. Meteorol. Soc.*, *135*, 1002–1019, doi:10.1002/qj.415.

Pinto, J. O. (1998), Autumnal mixed-phase cloudy boundary layers in the Arctic, *J. Atmos. Sci.*, *55*, 2016–2038.

Prenni, A. J., J. Y. Harrington, M. Tjernstrom, P. J. DeMott, A. Avramov, C. N. Long, S. M. Kreidenweis, P. Q. Olsson, and J. Verlinde (2007), Can ice-nucleating aerosols affect Arctic seasonal climate?, *Bull. Am. Meteorol. Soc.*, *88*, 541–550.

Pruppacher, H. R., and J. D. Klett (1997), *Microphysics of Clouds and Precipitation*, 2nd ed., Kluwer, Dordrecht, Netherlands.

Rauber, R., and A. Tokay (1991), An explanation for the existence of supercooled water at the top of cold clouds, *J. Atmos. Sci.*, *48*, 1005–1023.

Rogers, D. C., P. J. DeMott, and S. M. Kreidenweis (2001), Airborne measurements of tropospheric ice-nucleating aerosol particles in the Arctic spring, *J. Geophys. Res.*, *106*, 15,053–15,063.

Rosinski, J., and G. Morgan (1991), Cloud condensation nuclei as a source of ice-forming nuclei in clouds, *J. Aerosol Sci.*, *22*, 123–133.

Sheridan, L. (2008), Impact of the deposition coefficient and fall-speed relations on simulated cold clouds, M.S. thesis, 120 pp., Dep. of Meteorol., Penn State Univ., University Park.

Sheridan, L. M., J. Y. Harrington, D. Lamb, and K. Sulia (2009), Influence of ice crystal aspect ratio on the evolution of ice size spectra during vapor depositional growth, *J. Atmos. Sci.*, *66*, 3732–3743.

Shupe, M. D., and J. M. Intrieri (2004), Cloud radiative forcing of the Arctic surface: The influence of cloud properties, surface albedo, and solar zenith angle, *J. Clim.*, *17*, 616–628.

Turner, D. D., S. A. Clough, J. C. Liljegren, E. E. Clothiaux, K. Cady-Pereira, and K. L. Gaustad (2007), Retrieving liquid water path and precipitable water vapor from a radiation measurement (ARM) microwave radiometers, *IEEE Trans. Geosci. Remote Sens.*, *45*, 3680–3690.

Verlinde, J., et al. (2007), The Mixed-Phase Arctic Cloud Experiment (M-PACE), *Bull. Am. Meteorol. Soc.*, *88*, 205–221.

Walko, R. L., W. R. Cotton, M. P. Meyers, and J. Y. Harrington (1995), New RAMS cloud micro-physics parametrization. Part 1: The single-moment scheme, *Atmos. Res.*, *38*, 29–62.

Westbrook, C. D., R. J. Hogan, and A. J. Illingworth (2008), The capacitance of pristine ice crystals and aggregate snowflakes, *J. Atmos. Sci.*, *65*, 206–219.

Young, K. C. (1974), The role of contact nucleation in ice phase initiation in clouds, *J. Atmos. Sci.*, *31*, 768–776.

Zhang, G., G. McFarquhar, J. Verlinde, M. Poellot, and A. Heymsfield (2006), Contrasting properties of single-layer and multi-layer Arctic stratus sampled during the Mixed-Phase Arctic Cloud Experiment, in paper presented at 16th ARM Science Team Meeting, U.S. Dep. of Energy, Albuquerque, N. M.

A. Avramov, NASA Goddard Institute for Space Studies, 2880 Broadway, New York, NY 10025, USA. (aavramov@giss.nasa.gov)

J. Y. Harrington, Department of Meteorology, Pennsylvania State University, University Park, PA 16802, USA.